AD-A066 791 MARYLAND UNIV COLLEGE PARK DEPT OF AEROSPACE ENGINEERING F/G 20/5
NAVIER-STOKES SOLUTIONS FOR CHEMICAL LASER FLOWS: STEADY AND UN--ETC(U)
JAN 79 A P KOTHARI, E JONES, J D ANDERSON N00014-77-C-0257

UNCLASSIFIED NL

| OF |
AD
A066791

END
DATE
FILMED
5-79
DDC

SECURITY CLASSIFICATION OF THIS PAGE (When Data Entered)

(12)

REPORT DOCUMENTATION PAGE	READ INSTRUCTIONS BEFORE COMPLETING FORM
1. REPORT NUMBER	2. GOVT ACCESSION NO. 3. RECIPIENT'S CATALOG NUMBER
4. TITLE (and Subtitle) (6) Navier-Stokes Solutions for Chemical Laser Flows: Steady and Unsteady Flows	5. TYPE OF REPORT & PERIOD COVERED 6. PERFORMING ORG. REPORT NUMBER
7. AUTHOR(s) A.P. Kothari, J.D. Anderson, Jr., and E. Jones	8. CONTRACT OR GRANT NUMBER(s) N00014-77-C0257
9. PERFORMING ORGANIZATION NAME AND ADDRESS Department of Aerospace Engineering University of Maryland College Park, Maryland 20742	10. PROGRAM ELEMENT, PROJECT, TASK AREA & WORK UNIT NUMBERS NR061-248
11. CONTROLLING OFFICE NAME AND ADDRESS Office of Naval Research Code 438 Arlington, Virginia	12. REPORT DATE (11) January 1979 13. NUMBER OF PAGES 15
14. MONITORING AGENCY NAME & ADDRESS (if different from Controlling Office) ONR Resident Representative Johns Hopkins Univ., Rm. 358, Garland Hall Baltimore, Maryland 21218	15. SECURITY CLASS. (of this report) UNCLASSIFIED 15a. DECLASSIFICATION/DOWNGRADING SCHEDULE

16. DISTRIBUTION STATEMENT (of this Report)

Approved for Public Release; distribution unlimited

(15) N00014-77-C-0257

17. DISTRIBUTION STATEMENT (of the abstract entered in Block 20, if different from Report)

(10) Ajay P./Kothari, Everett/Jones
John D./Anderson, Jr.

DDC RECEIVED APR 3 1979 C

18. SUPPLEMENTARY NOTES

(12) 17 p.

19. KEY WORDS (Continue on reverse side if necessary and identify by block number)

Navier-Stokes solutions
Computational Fluid Dynamics
Unsteady Supersonic Mixing
Chemical Lasers

20. ABSTRACT (Continue on reverse side if necessary and identify by block number)

Time-dependent finite-difference solutions of the two-dimensional Navier-Stokes equations, fully coupled with the appropriate finite-rate chemical kinetic equations, are obtained for HF chemical laser flows. These solutions demonstrate the practicality of Navier-Stokes solutions for chemical laser flows. Results are given for steady flows where large pressure gradients are calculated as a natural part of the Navier-Stokes solutions. In addition, the effect of unsteady fluctuations intentionally introduced at the cavity inlet are studied. Such unsteady mixing increases the laser gain by more than a factor of two.

DD FORM 1 JAN 73 1473 EDITION OF 1 NOV 65 IS OBSOLETE

UNCLASSIFIED

SECURITY CLASSIFICATION OF THIS PAGE (When Data Entered)

79-0009

Navier-Stokes Solutions for Chemical Laser Flows: Steady and Unsteady Flows

A.P. Kothari, J.D. Anderson, Jr., and E. Jones, *University of Maryland, College Park, Md.*

17th AEROSPACE SCIENCES MEETING

New Orleans, La./January 15-17, 1979

NAVIER-STOKES SOLUTIONS FOR CHEMICAL LASER FLOWS: STEADY AND UNSTEADY FLOWS

Ajay P. Kothari,* John D. Anderson, Jr.,** and Everett Jones***
University of Maryland
College Park, Maryland

Abstract

Time-dependent finite-difference solutions of the two-dimensional Navier-Stokes equations, fully coupled with the appropriate finite-rate chemical kinetic equations, are obtained for HF chemical laser flows. These solutions demonstrate the practicality of Navier-Stokes solutions for chemical laser flows. Results are given for steady flows where large pressure gradients are calculated as a natural part of the Navier-Stokes solutions. In addition, the effect of unsteady fluctuations intentionally introduced at the cavity inlet are studied. Such unsteady mixing increases the laser gain by more than a factor of two.

Nomenclature

c	speed of light
C_i	mass fraction of species i
C_p	specific heat for constant pressure
C_v	specific heat for constant volume
D_{ij}	binary diffusion coefficient ($D_{ij}=D_{ji}$)
D_{im}	multicomponent diffusion coefficient for species i
E	total internal energy of the mixture
e	internal energy of the mixture
e_k	internal energy of the species k
$F_{v,J}$	vibrational-rotational interaction parameter - I
H	total enthalpy of the mixture
h	width of the nozzle
h_k	enthalpy of species k
h	Planck's constant
J	rotational quantum number
k	thermal conductivity of the mixture; Boltzmann constant in Eqs. (11), (21)-(23)
M	molecular weight
N_A	Avogadro's number
p	pressure
R	specific gas constant
R	universal gas constant
$\lvert R_v^{v+1}\rvert^2$	vibrational contribution to the electric dipole moment
T	temperature
t	independent time coordinate
$\bar{U},\bar{F},\bar{G},\bar{K}$	column matrices based on flow properties
u	x component of the velocity vector
U_r	reference velocity
v	y component of the velocity vector
x,y	independent spatial coordinates
$[i]$	concentration of species i
$\alpha_{v,J}$	small signal gain coefficient
ε	characteristic energy of interaction between a pair of molecules
η	mixture viscosity
ν_{kx}	x component of diffusion velocity for species k
ν_{ky}	y component of diffusion velocity for species k
σ	collision diameter of molecules, Å
ρ	density of the mixture
ρ_k	density of species k
$\dot{\omega}_k$	species production term due to chemical reactions

I. Introduction

The past decade has initiated the age of high energy lasers, first starting in 1966 with gasdynamic laser, and closely followed by breakthroughs in large chemical and electric discharge lasers. The gasdynamic laser, which generates its laser medium by means of a vibrational nonequilibrium nozzle expansion, is the subject of a recent book.[1] The electric discharge laser, which generates its laser via electron-atom and/or molecule collisions in a flow discharge, has been reviewed by Reilly[2]. The supersonic diffusion chemical laser, which obtains a laser medium from the products of chemical reaction, is nicely described in a review by Warren[3]. All of the above lasers involve the high speed flow of large amounts of gas, hence, they all involve the realms of aerodynamics and gasdynamics. For example, the HF or DF supersonic diffusion chemical laser involves the supersonic mixing of two dissimilar streams, as shown in Fig. 1.

Concurrently, the discipline of computational fluid dynamics has become a third-dimension in aerodynamics, complementing both laboratory experiments and pure analysis[4-6]. Work is advancing on both numerical methods and applications to practical engineering problems. The present paper is in the latter vein. Specifically it deals with the direct application of computational fluid dynamics to the solution of chemical laser flows.

The present paper represents a new, third generation of supersonic diffusion chemical laser analyses. First generation studies are exemplified by the RESALE computer program[7] (which assumes one-dimensional premixed flow) and the approximate flame-sheet model of Hofland and Mirels[8,9].

*Graduate Research Assistant, Dept. of Aerospace Engineering. Student Member AIAA.
**Professor and Chairman, Dept. of Aerospace Engineering. Associate Fellow, AIAA.
***Associate Professor, Dept. of Aerospace Engineering. Member AIAA.

Second generation studies involve more detailed fluid dynamic calculations, such as the boundary--layer solutions of King and Mirels[10] and Tripodi et.al[11]. The present investigation is a third generation study which incorporates the solution of the complete Navier-Stokes equations[13] for chemical laser flows for both the steady and unsteady inlet conditions. The full Navier-Stokes equations are able to model and solve the complicated chemically reacting, recirculating and separated flow regions at the base of chemical--laser nozzles -- an important aspect that affects chemical-laser performance, as emphasized by Grohs[12]. The advantage of invoking the Navier Stokes equations is that such complicated separated flow fields as well as any lateral or longitudinal pressure gradients induced by the chemical heat release are modeled exactly. The apparent disadvantage is that numerical solutions of Navier Stokes solutions take a long computer time but this can be reduced considerably per run if while doing parametric studies the runs are made back to back and the final steady state condition of one run is used as the initial condition for the other run with slightly different inlet conditions.

The purpose of the present paper is to assess the viability of Navier Stokes solutions for both the steady and unsteady chemical laser flows, and to underscore advantages as well as the present day restrictions of such numerical solutions. A second purpose of this paper is to compare the results obtained before and after the kinetics are switched on, i.e. to compare cold and hot flows. This numerical experiment graphically demonstrates the effects of chemical reaction on the laser fluid dynamics. Such considerations are important when extrapolating non-reacting supersonic mixing results obtained in the laboratory to the case of real chemical lasers.

Thirdly and more importantly it is the purpose of the present paper to illustrate the enhancement of mixing and gain obtained due to intentional fluctuations of the inlet conditions. To date, the use of the time-dependent method has been to obtain steady chemical laser flowfields as the asymptotic result of large times; the final steady--state flow has been the desired result, and the time-dependent technique has been simply a means to that end[14,34]. However, the work described in this paper takes advantage of the time-dependent Navier-Stokes solutions to study the transient effects of unsteady fluctuations in the flow properties at the cavity inlet on overall chemical laser performance downstream. In particular, the results show that intentional fluctuations in the inlet velocity vector can result in increased mixing and at least a factor of two increase in HF chemical laser gain. This paper presents the first results of such unsteady mixing phenomena in chemical lasers.

II. Physical Problem

Consider the parallel supersonic mixing of a stream of partially dissociated flourine with a stream of diatomic hydrogen, both diluted to some extend with He, as shown in Fig. 1. In the mixing region downstream of the nozzle exits, the following hypergolic chemical reactions take place.

Cold reaction:

$$F + H_2 \rightarrow HF^* (v) + H \qquad (1)$$

Hot reaction:

$$F_2 + H \rightarrow HF^* (v) + F \qquad (2)$$

which result in the direct formation of vibrationally excited HF as a reaction product. Over certain regions of the flow, a total population inversion may exist, i.e. $N_{HF(v+1)} > N_{HF(v)}$, where $N_{HF(v)}$ is the population of the vth vibrational level in HF. It is a population inversion that makes a chemical laser work (see Refs. 1 and 20 for background on laser properties). In a chemical laser, this inversion may be total, as previously described, or partial, where the inversion is carried by the rotational distributions.[1]

In the present investigation, the chemically reacting flowfield in Fig. 1 is solved by means of the complete two-dimentional Navier-Stokes equations. The mixing is assumed to be completely laminar. Multicomponent diffusion is treated in an exact fashion. Both the hot and cold HF reactions are included, and vibrational populations up to the $v = 8$ level in HF are calculated

The parallel mixing of Fig. 1 was chosen for solution because a) it consitutes a reasonably straightforward test of the present Navier-Stokes solutions; b) other results exist for this model and hence can be used for comparison; and c) it is a relatively uncomplicated model to compare results for hot and cold flows.

For the case of unsteady flow, basically the same flow configuration was used except that the flow conditions at the inlet now were varied in time instead of keeping them constant. In the case of oscillations in the y component of velocity at the inlet, the flow is off course not a parallel mixing flow although the time averaged value of v velocity was zero. Both the sinusoidal and sine square fluctuations at the inlet, firstly in the F_2 stream and then in both the streams are applied.

III. Analysis

A. Equations

Each of the nine HF vibrational levels is treated as a separate species interlinked by chemical and vibrational relaxation reaction. In addition to these nine HF vibrational-level species the reactants H, H_2, F, F_2 and an inert gas (diluent) He, make a total of 14 different species leading to 14 species continuity equations. These equations, in addition to the Navier Stokes equations viz. a) global continuity equation, b) x momentum equation, c) y momentum equation and d) energy equation yield a total of 18 equations. Non-dimensionalized, and in conservation form, they are

$$\frac{\partial}{\partial t}(\rho) + \frac{\partial}{\partial x}(\rho u) + \frac{\partial}{\partial y}(\rho v) = 0 \qquad (3)$$

$$\frac{\partial}{\partial t}\{\rho u\} + \frac{\partial}{\partial x}\{\rho u^2 + p + [\frac{2}{3}\mu(\frac{\partial u}{\partial x} + \frac{\partial v}{\partial y}) - 2\mu(\frac{\partial u}{\partial x})]$$

$$/Re_r + \frac{\partial}{\partial y}\{\rho uv - \mu(\frac{\partial v}{\partial x} + \frac{\partial u}{\partial y})/Re_r\} = 0 \qquad (4)$$

$$\frac{\partial}{\partial t}\{\rho v\} + \frac{\partial}{\partial x}\{\rho uv - \mu(\frac{\partial u}{\partial y} + \frac{\partial v}{\partial x})/Re_r\} + \frac{\partial}{\partial y}\{\rho v^2 + p$$

$$+ [\frac{2}{3}\mu(\frac{\partial u}{\partial x} + \frac{\partial v}{\partial y}) - 2\mu(\frac{\partial v}{\partial y})]/Re_r\} = 0 \qquad (5)$$

$$\frac{\partial}{\partial t}\{\rho E\} + \frac{\partial}{\partial x}\{\rho uH - \frac{1}{C_{prmg}} k \frac{\partial T}{\partial x} + \sum_{k=1}^{14} \rho_k h_k v_{kx}$$

$$+ \frac{u}{Re_r}[\frac{2}{3}\mu(\frac{\partial u}{\partial x} + \frac{\partial v}{\partial y}) - 2\mu \frac{\partial u}{\partial x}]$$

$$+ \frac{v}{Re_r}[-\mu(\frac{\partial v}{\partial x} + \frac{\partial u}{\partial y})]\} + \frac{\partial}{\partial y}\{\rho vH - \frac{1}{C_{prmg}} k \frac{\partial T}{\partial y}$$

$$+ \sum_{k=1}^{14} \rho_k h_k v_{ky} + \frac{u}{Re_r}[-\mu(\frac{\partial v}{\partial x} + \frac{\partial u}{\partial y})]$$

$$+ \frac{v}{Re_r}[\frac{2}{3}\mu(\frac{\partial u}{\partial x} + \frac{\partial v}{\partial y}) - 2\mu \frac{\partial v}{\partial y}]\} = 0 \qquad (6)$$

$$\frac{\partial}{\partial t}(\rho_k) + \frac{\partial}{\partial x}\{\rho_k(u + v_{kx})\} + \frac{\partial}{\partial y}\{\rho_k(v + v_{ky})\} =$$

$$= (\frac{h}{U_r \rho_r})\dot{\omega}_k$$

$$k = 1,2,\ldots.14 \qquad (7)$$

where

$$Re_r = \frac{\rho_r U_r h}{\mu_r} = \text{Reynolds number}$$

and

$$C_{prmg} = \frac{1}{P_{rr} Re_r (M_r)^2 (\gamma_r - 1)}$$

where

$$P_{rr} = \frac{\mu_r C_{pr}}{k_r} = \text{Prandtl number}$$

$$M_r = \frac{U_r}{\sqrt{\gamma_r R_r T_r}} = \text{Mach number}$$

$$\gamma_r = \frac{C_{pr}}{C_{vr}}$$

The previous equations are nondimensionalized as follows

$$t = \frac{t'}{h/U_r} \quad x = \frac{x'}{h} \quad y = \frac{y'}{h} \quad u = \frac{u'}{U_r}$$

$$v = \frac{v'}{U_r} \quad v_{kx} = \frac{v'_{kx}}{U_r} \quad v_{ky} = \frac{v'_{ky}}{U_r}$$

$$\rho_k = \frac{\rho'_k}{\rho_r} \quad \rho = \frac{\rho'}{\rho_r} \quad p = \frac{p'}{\rho_r U_r^2} \quad T = \frac{T'}{T_r}$$

$$k = k'/k_r \quad \mu = \mu'/\mu_r \quad h_k = h'_k/U_r^2$$

$$h = h'/U_r^2 \quad H = H'/U_r^2 \quad E = E'/U_r^2$$

where h is the characteristic width of the nozzle combination as shown in Fig. 1, subscript r refers to a characteristic reference value, and the primes refer to dimensional values.

Equation (3)-(7) can also be written as

$$\frac{\partial \bar{U}}{\partial t} + \frac{\partial \bar{F}}{\partial x} + \frac{\partial \bar{G}}{\partial y} = \bar{K} \qquad (8)$$

where $\bar{U}$, $\bar{F}$, and $\bar{G}$ are vectors with 18 components each, containing the terms in the curly brackets in Eqs. (3)-(7). Vector $\bar{K}$ contains the right-hand sides of Eqs. (3)-(7).

The remaining unknowns in Eqs. (3)-(7) are assumed to be related to p, T, and ρ_k in the following manner.

Species Internal Energy e_k

$$e_k = (e_{tran})_k + (e_{rot})_k + (e_{vib})_k + (e_{form})_k \qquad (9)$$

$$h_k = e_k + R_k T \text{ where } k = 1,2,\ldots.14 \qquad (10)$$

where $(e_{form})_k$ is the heat of formation of species k.

Calculation of Transport Properties

The transport properties viz. viscosity, thermal conductivity, and diffusion coefficients are first calculated for the individual species at given pressure and temperature and then obtained for the complete mixture for given concentrations.

Mixture viscosity: Viscosity for each species can be given by[2]

$$\eta = 0.000026693 \frac{1}{\sigma^2}\sqrt{\frac{M_k}{k}}\sqrt{\frac{kT/\epsilon}{\Omega^{(2,2)*}}} \qquad (11)$$

Here $\Omega^{(2,2)*}$ is a function of ϵ/kT and is related as

$$\frac{1}{\Omega^{(2,2)*}} = 0.697\,(1 + 0.323 \ln T^*) \qquad (12)$$

where $T^* = \varepsilon/kT$.

The vicosity of the mixture μ, is then obtained using the Wilke estimation method for gases at low pressure[22].

$$\mu = \sum_{i=1}^{6} \{\eta_i/[1 + \sum_{\substack{j=1 \\ j\neq i}}^{6} \phi_{ij} (\frac{y_j}{y_i})]\} \qquad (13)$$

where

$$\phi_{ij} = [1 + (\frac{\eta_i}{\eta_j})^{1/2}(\frac{M_j}{M_i})^{1/4}]^2/\sqrt{8}[1 + (\frac{M_i}{M_j})]^{1/2}$$

Thermal conductivity: The thermal conductivity of an individual species is related to the viscosity of the species in the following manner:

Monoatomic species[21]

$$\lambda' = (15/4)(R/M)\eta \qquad (14)$$

Diatomic species[21]

$$\lambda = \lambda'(1 + 0.88[(2/5)(C_p/R)-1]) \qquad (15)$$

Thermal conductivity for a mixture of gases at low pressure is given by[22]

$$k = \sum_{i=1}^{6} \{\lambda_i^*/[1+ \sum_{\substack{j=1 \\ j\neq i}}^{6} (\frac{M_{ij}}{M_i})^{1/2} \phi_{ij}(\frac{y_j}{y_i})]\}$$

$$+ \sum_{i=1}^{6} \{\lambda_i^{**}/[1 + \sum_{\substack{j=1 \\ j\neq i}}^{6} \phi_{ij}) \frac{y_j}{y_i})]\} \qquad (16)$$

where

$$\lambda_i^* = \lambda_i(1/[1+0.35(C_{pi}/R)-2)])$$

for H_2, F_2 and HF (diatomic species)
and $\lambda_i^* = \lambda_i$ for H, F, and He (monoatomic species),
also $\lambda_i^{**} = \lambda_i - \lambda_i^*$ for H_2, F_2, and HF,
$\lambda_i^{**} = 0$ for H, F, and He,
$M_{ij} = (M_i + M_j/2)$.

Diffusion coefficients: Treating each vibrational level of HF as a separate species, the binary diffusion coefficients are first obtained for all 14 species; these binary diffusion coefficients are independent of their concentrations.[22]

$$D_{ij} = 0.001858T^{3/2}[(M_i+M_j)/M_iM_j]^{1/2}/p\sigma_{ij}^2\Omega_D \qquad (17)$$

where p is the pressure in atmosphere, T is temperature in °K

$$\sigma_{ij} = (\sigma_i + \sigma_j)/2 \text{ in } \mathring{A}$$

Ω_D is the thermal collision integral

$$\Omega_D = f(kT/\varepsilon_{12})$$

where

$$\varepsilon_{12}/k = [(\varepsilon_1/k) \times (\varepsilon_2/k)]^{1/2}$$

variation of Ω_D with kT/ε_{12} is available in a tabular form.

The 196 (14 x 14) binary diffusion coefficients were used to yield multicomponent diffusion coefficients[22] D_{im}.

$$D_{im} = \frac{1 - y_i}{[\sum_{\substack{j=1 \\ j\neq 1}}^{n} (y_j/D_{ij})]} \qquad (18)$$

Species diffusion velocities (or diffusion mass flux) is related to concentration gradient by Fick's law.

$$\rho_i v_i = -\rho D_{im} \nabla C_i \qquad (19)$$

Chemical Production Term $\dot{\omega}_i$:

The species production term was calculated explicitly. Treating each vibrational level of HF as a separate species, 100 elementary reactions were obtained from the reactions given in Table VIII Ref. 23. These reactions involve chemical pumping, dissociation, and V-V and V-T vibrational transfers. The vibrational levels of H_2 were not treated separately, unlike Ref. 23.

The equilibrium constants as a function of temperature were obtained from the JANAF Tables[24] for the dissociation reactions. For the chemical pumping and V-V and V-T transfers, they were assumed to be of the form

$$K_{eq} = \exp[-(E_v - E_o)/RT]$$

where the reaction is $HF(0) \rightleftharpoons HF(v)$ and $E_v - E_o$ is the energy of the vth level above the ground state. The backward rate constants, k_b were then obtained from $k_b = K_{eq}/k_f$, where k_f is the forward rate constant obtained from Ref. 23.

Therefore, the finite-rate chemically reacting model consists of 100 elementary reactions involving 14 species. Hence, 14-species rate equations are written, one of which is given below for an example.

$$\frac{d}{dt}[HF(1)] = [k_{-31}[H][F] - k_{31}[HF(1)])[M_6]$$

$$+(K_{4a}[F][H_2] - 3k_{4a}[HF(1)][H])$$

$$+(K_{5b}[H][F_2] - k_{-5b}[HF(1)[F])$$

$$+(k_{-6a}[HF(0)] - k_{6a1}[HF(1)])[M_7]$$

$$+(k_{6a2}[HF(2)]-k_{-6a2}[HF(1)])[M_7]$$

$$+(k_{-6b1}[HF(0)]-k_{6b1}[HF(1)])[M_8]$$

$$+(k_{6b2}[HF(])]-K_{-6b2}[HF(1)])[M_8]$$

$$+(k_{-6c1}[HF(0)]-k_{6b1}[HF(1)])[M_9]$$

$$+(k_{6c2}[HF(2)]-k_{-6c2}[HF(1)])[M_9]$$

$$+(k_{-6d1}[HF(0)]-k_{6d1}[HF(1)])[M_{10}]$$

$$-(k_{6d2}[HF(2)]-k_{-6d2}[HF(1)])[M_{10}]$$

$$+(k_{6f1}[HF(0)]-k_{-6f1}[HF(1)])[M_5]$$

$$+(k_{6f2}[HF(2)]-k_{-6f2}[HF(1)])[M_5]$$

$$+(k_{-6g1}[HF(0)]-k_{6g1}[HF(1)])[M_4]$$

$$+(k_{6g2}[HF(])]-k_{-6g2}[HF(1)])[M_4]$$

$$+2(k_{-7a1}[HF(0)][HF(2)]-k_{7a}[HF(1)]^2)$$

$$+(k_{7a}[HF(2)]^2-k_{-7a2}[HF(1)][HF(1)]^2)$$

$$+(k_{-7b}[HF(3)][HF(0)]-k_{7b}[HF(1)][HF(2)])$$

$$+(k_{7b}[HF(2)][HF(3)]-k_{-7b2}[HF(1)][HF(4)])$$

$$+(k_{-7c1}[HF(0)][HF(4)]-k_{7c}[HF(1)][HF(3)])$$

$$+(k_{7c}[HF(2)][HF(4)]-k_{-7c2}[HF(1)][HF(5)])$$

$$+(k_{-7d1}[HF(0[][HF(5)]-k_{7d}[HF(1)][HF(4)])$$

$$+(k_{7a}[HF(2)[HF(5)-k_{-7d}[HF(1)][HF(6)])$$

B. Gain Calculations

For the low-pressure levels that exist in the mixing region, Doppler line broadening is assumed. Rotational equilibrium is assumed to exist, and only the P-branch laser transitions are considered. Then the optical small signal gain coefficient at line center has the value of[19]

$$\alpha_{v,J} = A(C_{v+1} - \lambda C_v) \tag{20}$$

where

$$A = \frac{\pi^{5/2} N_A^{1/2} |R_v^{v+1}|^2 J F_{vJ} \rho}{3(2kM_{HF}/\hbar c)^{1/2} Q(v+1) T^{1/2}} \tag{21}$$

$$\exp - \left[\frac{E(v+1,J-1)\hbar c}{kT}\right]$$

$$\lambda = \frac{Q(v+1)}{Q(v)} \exp - [E(v,J)-E(v+1,J-1)\hbar c/kT \tag{22}$$

$C_v = \rho_{HF(v)}/\rho \equiv$ mass fraction

$$Q(v) = \sum_{j=0}^{\infty} (2J+1)\exp-[E(v,J)\hbar c/kT] \tag{23}$$

= rotational partition function

$$E(v,J) = 20.95J(J+1) - 0.796J(J+1)(v+1/2)cm^{-1} \tag{24}$$

= vibrational-rotational energy

The average integrated gain in the y direction can be obtained as

$$G_{v,J} = \frac{1}{h} \int_0^h \alpha_{v,J}\, dy \tag{25}$$

C. Boundary Conditions

A comment is made on the boundary conditions at y = 0 and y = h. Symmetry conditions hold at these boundaries, as can be seen from Fig. 1, which models a segment of the multinozzle flow characteristic of many chemical lasers, i.e.

$$\frac{\partial u}{\partial y} = \frac{\partial p}{\partial y} = \frac{\partial T}{\partial y} = \frac{\partial \rho i}{\partial y} = v = 0$$

at y = 0 and h. In the present finite-difference scheme, the reflection principle is used; this is an accurate representation of boundary conditions on a line of symmetry, i.e.

$$p_{j+1} = p_{j-1} \quad T_{j+1} = T_{j-1} \quad V_{j+1} = -V_{j-1} \text{ etc.}$$

where j is an index in y direction and j lies on the boundary itself.

IV. Numerical Solution

A time dependent technique patterned after the MacCormack[25] approach was employed to generate the steady-state solution.

Equation (8) can be written in the following form,

$$\frac{\partial \bar{U}}{\partial t} = -\frac{\partial \bar{F}}{\partial x} - \frac{\partial \bar{G}}{\partial y} + \bar{K} \tag{26}$$

If the distribution of flowfield variables is specified at any instant of time (say n), the spatial gradients of $\partial\bar{F}/\partial x$ and $\partial\bar{G}/\partial y$ can be calculated at every grid point by finite differences, and the vector $\bar{K}$ can be explicitly computed from the known temperature, rate constants, and concentrations. In turn, the time derivative $\partial\bar{U}/\partial t$ can be computed from Eq. (26). This allows the computation (in principle) of new values at time (n+1) by

$$\bar{U}^{n+1} = \bar{U}^n + \left(\frac{\partial \bar{U}}{\partial t}\right)_n \Delta t \tag{27}$$

The components of the new vector $\bar{U}^{n+1}$ then specify all the properties at a grid point one step ahead in time. Steady state is essentially attained when $\partial\bar{U}/\partial t$ approaches zero. However,

Eq. (27) is of first-order accuracy only. In contrast, MacCormack uses a predictor-corrector method of second-order accuracy. It involves the generation of intermediate predicted values at time (n+1) via Eq. (28). Then these predicted values are used again in the conservation equation in a "corrector" fashion to obtain values at time (n+2). Averaging of these two steps leads to a higher accuracy at time (n+1) as shown in Eq. (30). This process as applied to mixing flows is described in more detail in Ref. 26.

$$\bar{U}^{n+1} = \bar{U}^{n} + \left[-\frac{\partial \bar{F}}{\partial x} - \frac{\partial \bar{G}}{\partial y} + \bar{K}\right]_{n} \Delta t \qquad (28)$$

$$\bar{U}^{n+2} = \bar{U}^{n+1} + \left[-\frac{\partial \bar{\bar{F}}}{\partial x} - \frac{\partial \bar{\bar{G}}}{\partial y} + \bar{\bar{K}}\right]_{n+1} \Delta t \qquad (29)$$

and

$$\bar{U}^{n+1} = \bar{U} + \frac{\bar{U}^{n+2} - \bar{U}^{n}}{2} \qquad (30)$$

Here n refers to the time step and the title refers to intermediate values.

The vectors $\bar{F}$ and $\bar{G}$ contain spatial gradients of temperature and velocities directly and of species densities indirectly through the diffusion velocities. In turn, spatial gradients of vectors $\bar{F}$ and $\bar{G}$ themselves need to be taken to solve Eqs. (28) and (29). Thus, effectively, spatial gradients of the thermodynamic quantities need to be taken to a largest order of two. This offers various combinations of forward, backward, and central differencing schemes to compute the spatial derivatives, a detailed discussion of which appears in Ref. 14. In the present paper, the following differencing scheme was used; it is shown in Ref. 14 to be the most appropriate scheme for the mixing flows of present interest.

Forward differencing is used on the $\bar{F}$ and $\bar{G}$ vectors to obtain the intermediate properties (predictor step), e.g.

$$\frac{\partial \bar{F}}{\partial x}(2,j,k) = \frac{\bar{F}(3,j,k) - \bar{F}(2,j,k)}{\Delta x} \qquad (31)$$

Backward differencing is used for the corrector step, e.g.

$$\frac{\partial \bar{G}}{\partial y}(i,2,k) = \frac{\bar{G}(i,2,k) - \bar{G}(i,1,k)}{\Delta y} \qquad (32)$$

However, a reverse combination, viz. backward differencing for predictor step and forward differencing for the corrector step, is used for the gradients of T, u, v, ρ, and ρ_k. This is termed the "Modified MacCormack" approach in Ref. 14.

The time step used to advance the solution in time is the minimum of the time steps due to the CFL criteria[27] and the characteristic relaxation time. Here, the CFL criteria are given by the minimum of

$$\Delta t = \Delta x/(u+a) \text{ and } \Delta t = \Delta y/(v+a)$$

whereas the chemical relaxation time is given as[28]

$$\tau = -1/\frac{d[\dot{\omega}_i]}{d[\omega_i]}$$

A 9 x 9 grid size (81 mesh points) is used.

V. Results and Discussion

A. Steady Flow

Solutions are obtained for the flow depicted in Fig. 1. At time t = 0, the initial conditions are rather aribtrarily chosen as constant properties in each of streams 1 and 2 (same as the upstream boundary conditions at the nozzle exits held fixed with time).

Consider the point defined by x/h = 10.0 and y/h = 0.375. The time history of the static temperature at this point is given in Fig. 2. Cold-flow calculations (the fluid dynamics without the chemical reactions) are made through a nondimensional time of 24 to allow the two streams to partially mix. After this time, hot-flow calculations (the fluid dynamics fully coupled with the chemical kinetics) are made. Note from Fig. 2 that the switch to a hot flow causes a discontinuous increase in dT/dt, and a subsequent approach to a higher steady-state temperature. For comparison, the purely cold-flow case is carried out to a steady state, as also shown in Fig. 2. Note that the combined effect of chemical reactions and vibrational relaxation lead to a 35% increase in static temperature in comparison to the purely aritifical cold-flow case.

Steady-state profiles of velocity, pressure, and temperature with respect to y/h are given in Figs. 3, 4, and 5, respectively. In each figure, results for the longitudinal stations x/h = 0,5 and 10 are given. Also in each figure, the solid and dashed lines correspond to hot and cold flow, respectively. Note from Fig. 3 that, in contrast to temperature, the velocity profiles downstream of the nozzle exits show little influence due to chemical reactions -- a result that is almost classical in most high-temperature gasdynamic problems. Also note that the slower-moving stream of H_2 is accelerated more than the faster-moving stream of F and F_2 is retarded, due to the mixing process. The pressure variations, which are plotted on an expanded scale in Fig. 4, show virtually a constant pressure in the y direction, except for a small variation in the middle of the mixing zone. For hot flow, there is an adverse pressure gradient in the flow direction; in contrast the net effect of the purely fluid dynamic mixing appears to be a slight favorable pressure gradient, at least for the first 10 nozzle heights downstream. The corresponding temperature profiles are shown in Fig. 5. Comparing the cold-flow profiles, it is apparent that the viscous shear action causes a larger local temperature rise in the mixing region at x/h = 5.0 than at x/h = 10 because y gradients of velocity are larger near the nozzle exits. However, in going from x/h = 5.0 to x/h = 10.0, the mean temperature rise is more over the whole cross section whereas the peak temperature of the faster streams seems to drop because the interface streamline would bend toward the slower stream. The average pressure also slightly decreases

as the flow moves downstream, as noted in Fig. 4. In contrast, the hot flow profiles clearly show an almost discontinuous increase in the temperature, a fact already noted from Fig. 2.

Figures 6 and 7 illustrate density profiles of various HF vibrational levels at x/h = 5 and 10, respectively. The growth of the reaction zone can be seen clearly. Total population inversions exist between vibrational level increases as the flow moves downstream, the small signal gain does not necessarily increase since the absolute difference between the densities of HF(0), HF(1), and HF(2) does not always increase.

The calculated growth of the reaction zone, as defined by the region where $\rho_{HF(0)}$ is greater than 10% of the maximum value, is shown in Fig. 8. This figure is taken from Ref. 12, and contains experimental data taken at TRW. The present results are marked on Fig. 8 and show the same laminar variation as the experimental data.

The existence of population inversions and hence laser action is best seen in Fig. 9, where densities of various HF vibrational levels at $y/h = 0.375$ are plotted with respect to x. Inversions exist between the 0-1 levels and 1-2 levels, which yields the small-signal gain $a_{v,J}$ as calculated by Eq. (20). These gains are shown in Figs. 10 and 11. Figure 10 shows the variation of the small signal gain with respect to x at $y/h = 0.375$ for the vibrational level transition 1-0 for various rotational levels (only P-branch transitions are assumed). Figure 11 shows similar results for the 2-1 transition. The values of gain and the spatial extent of the lasing region as indicated on Fig. 10 and 11 are typical of conventional HF chemical lasers, as obtained from Refs. 18 and 19.

A few words about stability and convergence are in order. The present time-dependent calculations smoothly and regularly approach a steady-state solution as long as the requisite stability criteria are followed; i.e., the solutions are stable as long as the time increment is less than the CFL and chemical relaxation times. With regard to convergence, the question can be asked: Is enough accuracy obtained with the present 9 x 9 grid, which at first glance appears rather coarse? An answer is given in Fig. 12. Here, the final steady-state temperature at x/h = 5 and y/h = 0.75 is given for three different grid sizes: 5 x 5, 9 x 9 and 13 x 13. It appears that a 9 x 9 grid is sufficiently accurate, and that a further definition by more grid points is unnecessary. This is totally consistent with time-dependent solutions of of other problems[1,29-31] where sufficient accuracy has been obtained with seemingly very coarse grids. Apparently, the time-dependent mechanism is "self-correcting" at each time step, allowing the physics contained in the conservation equations to bear more strongly and accurately at each grid point. The philosophical point not withstanding, experience has clearly proven that time-dependent solutions require fewer grid points than might be expected for steady-state analyses. The present results are a case in point. As long as the cell Reynolds number in the y direction is on the order of unity, the gradients are adequately accounted for, as in the present calculations.

The present Navier-Stokes calculations are compared with the results of King and Mirels[19] and LAMP[18] in Figs. 13 - 15. Both Refs. 18 and 19 are boundary-layer solutions. King and Mirels[19] assume two semi-infinite streams; hence, the pressure is assumed constant in both the x and y directions. The LAMP program calculates a pressure gradient in the x direction by means of a quasi-one-dimensional heat-addition approximation, but assumes constant pressure in the y direction. The present Navier-Stokes calculations allow pressure gradients in any direction. The authors express their extreme appreciation to Dr. Walter Glowacki of the Naval Surface Weapons Center (White Oak, Md.) for his running of the LAMP code for comparison with the present work.

The case shown in Figs. 13-15 is a strongly reacting mixture, with conditions at the nozzle exit of (see Fig. 1 for the nomenclature) p = 5 Torr, $T_1 = 110^{\circ}K$, $T_2 = 400^{\circ}K$, $u_1 = 1400$ m/sec, $u_2 = 2140$ m/sec. In stream 1, $\rho_{H_2} = 1.47 \times 10^{-3}$ kg/m^3. In stream 2, $\rho_F = 1.1 \times 10^{-3}$ kg/m^3 and $\rho_{H_e} = 5.7 \times 10^{-4}$ kg/m^3. This mixture is so strongly reacting that a large adverse pressure gradient is produced in the flow firection; note from Fig. 13 that both the present calculations and LAMP predict approximately a factor of five pressure increase in a distance on the order of a centimeter. In fact, the changes are so severe that the LAMP calculation experienced some spurious wiggles, and then blew up beyond 0.8 cm. (However, this in no way reflects on the viability of LAMP, because no subsequent efforts were made to adjust grid size, etc., to attempt to overcome this behavior.) Nevertheless, the comparison between LAMP and the present calculations is reasonable; in contrast, the constant pressure assumption of King and Mirels[19] is not valid for this case. Similar comparisons for T and HF variations are given in Figs. 14 and 15, respectively.

Return to the conditions given in Fig. 1. Here, the densities of F_2, F and H are relatively small -- a dilute case. The results of Figs. 2-11 apply to this case. In turn, these results are compared with a calculation from LAMP in Fig. 16. The profiles of HF(0) and T are shown as a function of y at x/h = 10. Note that the LAMP results predict peak temperatures and HF densities that are about 20 and 70% higher, respectively, than the present calculations. This is considered to be reasonalbe agreement in light of the different kinetic rates and transport properties in the two programs. The present results calculate detailed and variable transport properties at each point in the flow; lamp assumes constant Prandtl and Lewis numbers. Also, keep in mind that the pressure gradients in the two-dimensional flow appear quite naturally and exactly in the present Navier-Stokes formulation, whereas LAMP has an approximate calculation of pressure gradient and only in the x direction.

A word about computer time is also in order. For the present Navier-Stokes results, computer times of 30 and 90 min on a UNIVAC 1108 for the dilute and strongly reacting cases, respectively, were required. The cost averaged $350 per run. This is about three times more expensive than LAMP

for the same cases. However, keep in mind that the present time-dependent calculations start with initial conditions that are constant but different properties in streams 1 and 2, i.e., no mixing of the two streams. If more realisitc initial conditions are fed in, the computer time can be drastically reduced. In particular, if several different parametric runs are stacked together, and the initial conditions for one are taken as the solution from another, the running times should be comparable to or better than LAMP. This behavior is already observed in time-dependent calculations of gasdynamic laser performance,[32] where by stacking several runs, the running times of the second and remaining runs are one-fifth that of the first run. In this fashion, Navier-Stokes calculations can be made cost-effective; therefore, they are not inordinately long as may first be expected.

B. Unsteady flow

The main thrust of the present paper is to answer what happens if one (or more) of the variables at the inlet in one of the streams (or both streams) is fluctuated in line. Does it enhance or inhibit mixing and how does it affect gain?

It was observed that a time-wise sinusoidal variation in inlet pressure in the F_2 stream (and hence density, keeping the temperature constant) about a certain mean value failed to improve mixing. Correspondingly no better gain was observed. Variation in frequency and/or amplitude of the pressure fluctuation did not improve this situation.

Next, in order to vary the momentum of the incoming flow, the x-component of velocity was fluctuated about a mean value of 2000 m/sec. A noticeable effect of mixing was observed only for angular velcoity about 3×10^5 rad/sec and for a rather large amplitude of +500 m/sec. A plot of velocity vectors in the flow at a particular time indicated the presence of a large induced y-component of velocity in the flow due to coupling with the fluid dynamics, and this is perhaps responsible for increased mixing.

Therefore, all subsequent cases were run wherein only the sinusoidal variation of the y-component of velocity was intentionally forced at the inlet. This yielded a considerably improved mixing and also higher values for small signal and in particular the integrated gain. Many different cases were simulated of which a case with frequency $\omega = \pi \times 10^5$ rad/sec and an amplitude of $v = + 500$ m/sec yielded the most favorable results. For example, Figure 17 illustrates the transient variation of the F_2 density at a given point in the flow for three different amplitudes in the fluctuation of the inlet y-component of velocity (v), namely $\Delta v = + 5\%$, $+ 10\%$ and $+ 25\%$ of the x-component of velocity ($\bar{u}$). The horizontal dashed lines are the F_2 densities obtained from a previous steady-flow solution for the same inlet properties. Note that for $\Delta v = + 25\%$ the unsteady flow results in a time-mean F_2 density that is above the steady-flow value. These unsteady results, when integrated over time, lead to the results in Figure 18. Here, the flow-wise variation of time averaged density of F_2 is shown for various cases. This shows clearly the improvement in mixing due to the fluctuating of v at the inlet. Gain results also show the consequence of the enhancement of mixing. A rather remarkable factor of two increase in the integrated gain was obtained for the case outlined above (as discussed later).

It was further observed that oscillations of v in both the F_2 and H_2 streams at various different phase angles yielded results generally similar to or inferior to the fluctuations in only one stream.

It should be emphasized here that the frequency of oscillations was selected to be of such a magnitude so as to have wavelength of the order of the cavity length. Further parametric studies confirmed this hypothesis. The Strouhal number is of the order recommended in Ref. 33.

Figures 19 and 20 clearly indicate the remarkable superiority of unsteady mixing. All the results here have again been time averaged over a periodic time of one oscillation. Figure 19 shows, clearly, a larger and more spread out production of HF for the case of v velocity fluctuation than the other two plotted. Ability of the oscillation to populate the region of the flow for $y/h > 0.5$, which did not occur for the other two cases, in general produced integrated gain larger by a factor of two, thus making it possible to increase gain by a substantial amount. Figure 20 again shows various HF levels versus x for a constant value of y. Here again a faster mixing and faster pumping is clearly seen e.g. at $x/h = 2.5$.

Sine square [$\sin^2 \theta$] variation in the y-component of velocity was also simulated, thus yielding a definite value for the time averaged mean of a fluctuation. This suggested another case of non-parallel mixing of two steady streams at an angle (viz. $\Delta\theta = 14^0$) w.r.t. each other. Both these cases produced inferior mixing gain results. The shock waves produced in the later case accounted for a rise in temperature in the lasing region and hence faster V-V, V-T deactivation reactions, thus impeding gain.

The uniform profiles of velocity and concentrations of F and F_2 used at the inlet, although sufficient and proper for parametric studies at earlier time, need to be modified to account for no slip condition and catalytic recombination at the nozzle wall. Also a recirculation region is produced near the inlet due to finite thickness of nozzle walls. These questions are being addressed to, presently, using the Navier-Stokes equations to solve the flowfields. In particular the Boundary Layer profile in the x-component of velocity at the inlet in both streams has already been simulated. The final integrated gain results are shown in Figure 21 for P-transiion with V,J = 1,1 for various different aforementioned cases including the boundary layer case. The decrease in gain due to the presence of real effects like B. L. is easily seen. Integrated gain is plotted in Figs. 22 and 23. In Fig. 22 integrated gain plotted versus non-dimensional x-wise location clearly illustrates the increase in gain experienced due to the unsteadiness of the flow. For the case of transitions from vibrational levels 1 to 0. Again Fig. 23, which is a similar plot

for the vibrational level transition 2 to 1 reemphasizes the same point. In both these cases the gain is calculated from the various HF level species densities increased over a time period of the oscillation.

As a final comment on the fluid dynamic aspects of unsteady mixing, note that there is a physical improvement in mixing due to the forced intermingling of the fluid elements. This can be seen from Fig. 24a and b, which shows the time history of the particles inserted at two different times in the flow. The nonuniform particle paths clearly show the extent of material intermingling. These path lines were obtained as part of the computer results by means of a special subroutine.

V. Conclusions

The present paper introduces a "third generation" of chemical-laser analysis, i.e, Navier-Stokes solutions for the flowfield coupled with the detailed chemical kinetics for both the hot and cold reactions of HF for both steady and unsteady flows. The results for the steady flow are also described in Ref. 35. In particular, the present results show the following:

1. Navier-Stokes solutions for supersonic diffusion chemical lasers are indeed feasible; however, computer times equivalent to about 30 min or longer on a UNIVAC 1108 are required for a single case. By stacking cases back-to-back such that the initial conditions for one are obtained from the solution of another, the net time per case can be substantially reduced.

2. The major potential for such Navier-Stokes solutions is in the analysis of recirculation and separated flow effects on laser performance.

3. In a comparison between hot and cold flows the chemical reactions markedly affect the temperature distributions, but have little effect on the velocity distributions. The pressure increases in the flow direction due to chemical reactions, an effect to be expected from simple analogy with constant area heat addition in supersonic flows. In contrast, for cold flows, the longitudinal pressure variation is reasonably constant and may even decrease slightly.

4. The growth of the laminar reaction zone predicted in the present paper compares favorably with experiment.

5. Navier-Stokes calculations have the distinct advantage that the two-dimensional pressure gradients appear quite naturally and exactly. In strongly reacting cases, the proper accounting of these pressure gradients are absolutely necessary; the constant pressure boundary-layer assumption is not adequate.

6. Considering the differences between the physical properties and fluid dynamic modeling of the present Navier-Stokes analysis and LAMP, fairly reasonable agreement is obtained between the two. However, the constant pressure results of King and Mirels differ considerably, and are obviously not valid for cases where strong pressure gradients occur in the real problem.

7. It is the first numerical solution of the full Navier-Stokes equations with fully coupled kinetics for both the cold and hot reactions for HF and multicomponent diffusion for the case of inherently unsteady supersonic mixing flows.

8. It shows that the integrated gain for HF chemical lasers can be increased substantially by intentionally fluctuating the y-component of velocity at the inlet. This leads to better mixing and also higher gain in general.

9. Real effects like presence of bounary layer in velocity at inlet impeded mixing and hence reduces integral gain.

The authors recognize that the density variations created in the cavity by the fluctuations will have an adverse effect on the overall quality of the laser beam. However the purpose of this study has been to examine the fluid dynamic and chemical kinetic consequences of such fluctuations. The effect on beam quality is beyond the scope of the present paper.

Acknowledgment

This work was supported in part under ONR contract N00014-77-C-0257. Mr. Morton Cooper as contract monitor. Acknowledgment is also given to the Minta Martin Fund for Aeronautical Research, an endowment fund given to the College of Engineering, University of Maryland, by the late Glenn L. Martin. Support of the University of Maryland Computer Science Center is also gratefully acknowledged.

A special thanks also to Ms. Sue Osborn for the diligent effort in typing the manuscript.

References

[1]Anderson, J. D., Jr., Gasdynamic Lasers: An Introduction, Academic Press, New York, 1976.

[2]Reilly, J. P., "High Power Electric Discharge Lasers (EDL's)," Astronautics and Aeronautics, Vol. 13, March 1975, pp. 52-63.

[3]Warren, W. R., Jr., "Chemical Lasers," Astronautics and Aeronautics, Vol. 13, April 1975, pp. 36-49.

[4]Roache, P. J., Computational Fluid Dynamics, Hermosa Publishers, Albuquerque, N. Mex., 1972.

[5]Chapman, D. R., Mark, H., and Pirtle, M. W., "Computers vs. Wind Tunnels," Astronautics and Aeronautics, Vol. 13, April 1975, pp. 22-30.

[6]Taylor, T. D., "Numerical Methods for Predicting Subsonic Transonic and Supersonic Flow," AGARDograph No. 187, January, 1974.

[7]Emanuel, G., Adams, W. D., and Turner, E. B., "Resale 1: A Chemical Laser Computer Program," Aerospace Corp. TR-0172 (2276)-1, El Segundo, CA., March 1972.

[8]Hofland, R. and Mirels, H., "Flame-Sheet Analysis of CW Diffusion-Type Chemical Lasers, I. Uncoupled Radiation," AIAA Journal, Vol. 10, April 1972, pp. 420-428.

[9]Hofland, R. and Mirels, H., "Flame Sheet Analysis of CW Diffusion-Type Chemical Lasers, II. Coupled Radiation," AIAA Journal, Vol. 10, Oct. 1972, pp. 1271-1280.

[10]King, W. S. and Mirels, H., "Numerical Study of a Diffusion-Type Chemical Laser," AIAA Journal, Vol. 10, Dec. 1972, pp. 1647-1654.

[11]Tripodi, R., Coulter, L. J., Bronfin, B. R. and Cohen, L. S., "Coupled Two-Dimensional Computer Analysis of CW Chemical Mixing Lasers," AIAA Journal, Vol. 13, June 1975, pp. 776-784.

[12]Grohs, G. L., "Chemical Laser Cavity Mixing and Turbulence," AIAA Paper 76-56, Syracuse, N.Y., 1976.

[13]Schlichting, H., Boundary Layer Theory, McGraw-Hill, New York, 1968.

[14]Kothari, A. P. and Anderson, J. D., Jr., "Navier-Stokes Solutions for Chemical Laser Flows: Cold Flows," AIAA Journal, Vol. 14, May 1976, pp. 702-703; also AFOSR-TR-75-1447 (TR No. AE 75-6, Dept. of Aerospace Engineering, Univ. of Md., College Park, Md., June 1975).

[15]Butler, R. D. and O'Rourke, P. J., "A Numerical Method for Two-Dimensional Unsteady Reacting Flows," 16th International Symposium on Combustion, Aug. 15-21, 1976, Cambridge, Mass.

[16]Ramshaw, J. D., Mjolsness, R. C. and Farmer, O. A., "Numerical Method for Two-Dimensional Steady-State Chemical Laser Calculations," submitted to the Journal of Quantitative Spectroscopy and Radiative Transfer, March 1976.

[17]Rivard, W. C., Farmer, O. A., and Butler, T. D., "RICE: A Computer Program for Multicomponent Chemically Reactive Flows at All Speeds," Rept. LA-5812, Los Alamos Scientific Lab., N. Mex., Nov. 1974.

[18]Theones, J. and Ratcliff, A.W., "Chemical Laser Oscillator Analytical Model," AIAA Paper 73-644, Palm Springs, Calif., 1973.

[19]King, W. S., and Mirels, H., "Numerical Study of a Diffusion Type Chemical Laser," Aerospace Corporation SAMSO-TR-75-140, El Segundo, Calif., June 1975.

[20]Lengyle, B. A., Lasers, Wiley-Interscience, New York, 1971.

[21]Brokaw, R. S., "Alignment Charts for Transport Properties Viscosity, Thermal Conductivity and Diffusion Coefficients for Non-Polar Gases and Gas Mixtures at Low Density," NASA TR-R-81, 1961.

[22]Reid, R. C. and Sherwood, T. K., The Properties of Gases and Liquids, McGraw-Hill, 1966.

[23]Cohen, N., "A Review of Rate Coefficents for Reactions in the H_2F_2 Laser System," Aerospace Corporation Rept. TR-5073 (3420)-9, El Segundo, Calif., Nov. 1972.

[24]Stull, D. R. and Prophet, H., JANAF Thermochemical Tables, 2nd Edition, NSRDC-NBS 36, U.S. Dept. of Commerce, Washington, D.C., June 1971.

[25]MacCormack, R. W., "The Effect of Viscosity in Hypervelocity Impact Cratering," AIAA Paper, 69-354, Cincinnati, Ohio, 1969.

[26]Jones, E. and Anderson, J. D., Jr., "Numerical Solutions of the Navier-Stokes Equations for Laminar and Turbulent Supersonic Mixing Flows," Aerospace Engineering Technical Rept. AE-75-5, University of Maryland, College Park, Md., June 1975.

[27]Courant, R., Fredrichs, K. O. and Lewy, H., "Ueber die Diferentzengleichunger der Mathematischen der Matehmatischen Physic," Mathematics Annuals Vol. 100, 1928, p. 32.

[28]Vincenti, W. G. and Kruger, C. H., Introduction to Physical Gas Dynamics, Wiley, New York, 1965.

[29]Anderson, J. D., Jr., "A Time-Dependent Analysis for Vibrational and Chemical Nonequilibrium Nozzle Flows," AIAA Journal, Vol. 8, March 1970, pp. 545-550.

[30]Anderson, J. D., Jr., Albacete, L. M., and Winkelmann, A. E., "On Hypersonic Blunt Body Flow Fields Obtained with a Time-Dependent Technique," NOLTR-68-129, Aug. 1968, Naval Ordnance Lab., White Oak, Md.

[31]Moretti, G. and Abbett, M., "A Time-Dependent Computational Method for Blunt Body Flows," AIAA Journal, Vol. 4, Dec. 1966, pp. 2136-2141.

[32]Glowacki, W. J. and Anderson, J. D., Jr., "A Computer Program for CO_2-N_2-H_2O Gasdynamic Laser Gain and Maximum Available Power," NOLTR 71-210, Oct. 1971, Naval Ordnance Lab., White Oak, Md.

[33]Roshko, A., "Structure of Turbulent Shear Flows: A New Look," Dryden Lecture of AIAA; AIAA Paper 76-78, 1976. Also AIAA Journal, Vol. 14, No. 10, October 1976, pp. 1349-1357.

[34]Kothari, A. P. and Anderson, J. D., Jr., "Navier-Stokes Solutions for Chemical Laser Flows," Technical Report AE 75-6, Dept. of Aerospace Eng., University of Maryland, June 1975.

[35]Kothari, A. P., Anderson, J. D., Jr., and Jones, E., "Navier-Stokes Solutions for Chemical Laser Flows," AIAA Journal, Vol. 15, No. 1, Jan. 1977, pp. 92-100.

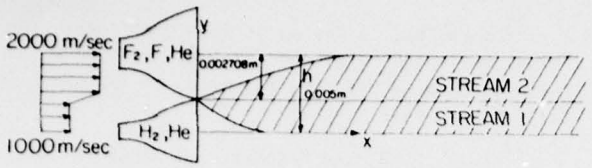

NOZZLE CONFIGURATION

	STREAM 1	STREAM 2
P n/m^2	500	500
T °K	150	150
ρ Kg/m^3	12862×10^{-3}	24514×10^{-3}
ρ_{F_2} Kg/m^3	—	73128×10^{-4}
ρ_{H_2} Kg/m^3	32328×10^{-4}	—
ρ_F Kg/m^3	—	24376×10^{-4}
ρ_H Kg/m^3	—	—
ρ_{He} Kg/m^3	96288×10^{-4}	14764×10^{-3}

INITIAL CONDITIONS
$\rho_k = 0$ for k = 6,7,----14

Figure 1

Geometric model and given cavity inlet conditions.

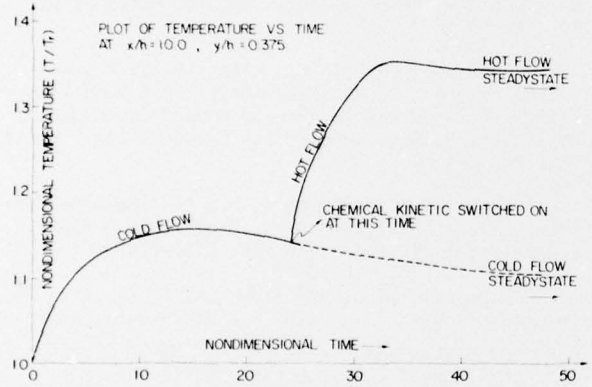

Figure 2

Transient variation of static temperature at x/h = 1.0 and y/h = 0.375.

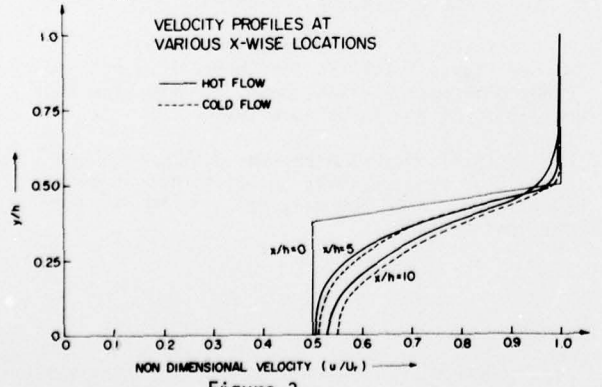

Figure 3

Steady-state velocity profiles at various x-wise locations.

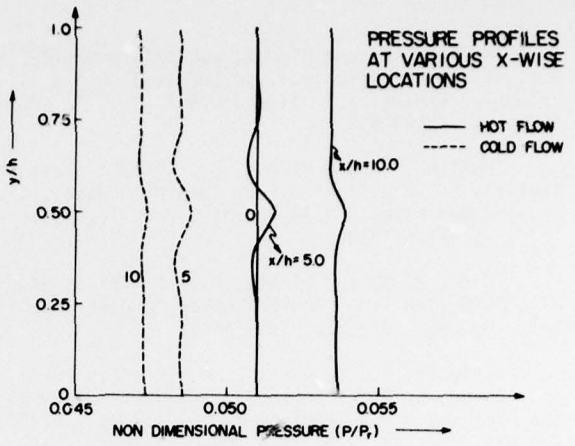

Figure 4

Steady-state pressure profiles at various x-wise locations.

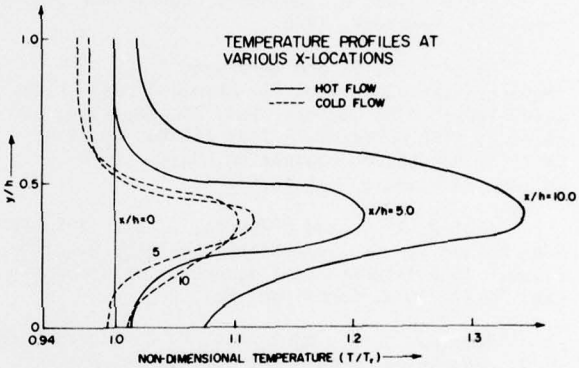

Figure 5

Steady-state temperature profiles at various x-wise locations.

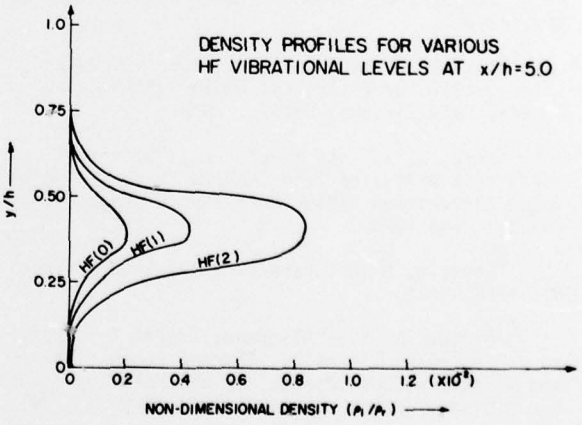

Figure 6

Steady-state density profiles for HF(v); x/h = 5.0.

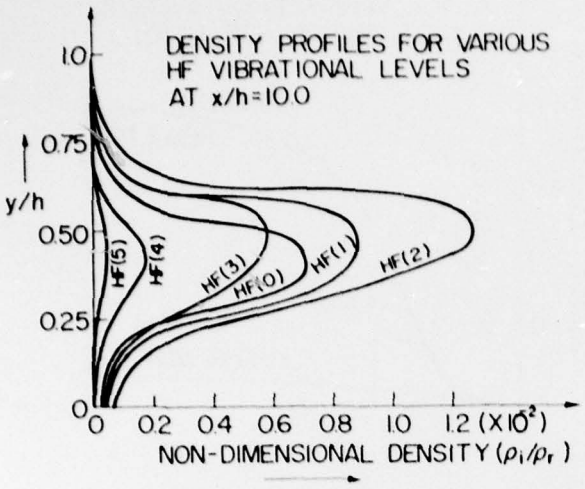

Figure 7

Steady-state density profiles for HF(v); x/h = 10.0.

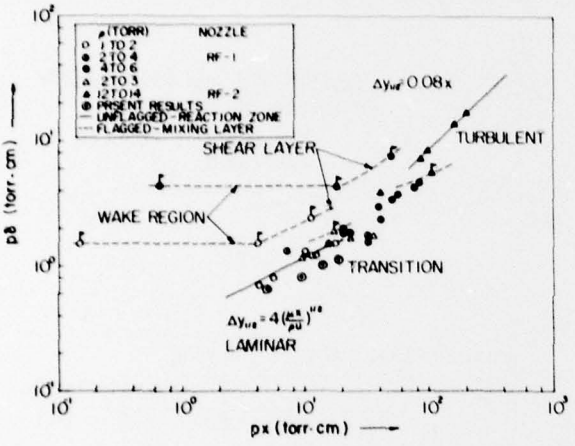

Figure 8

Growth of the reaction zone; comparison of present calculations with experiment (see Ref. 12).

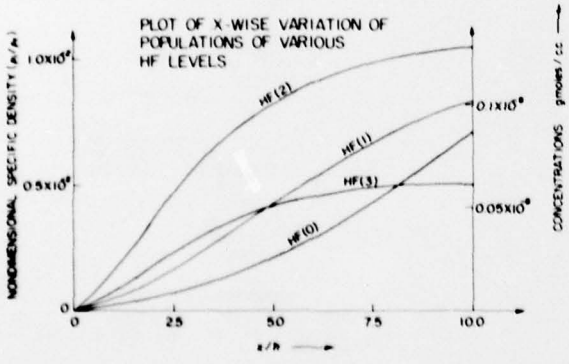

Figure 9

Variation of HF(v) ub the flow direction; y/h=0.375.

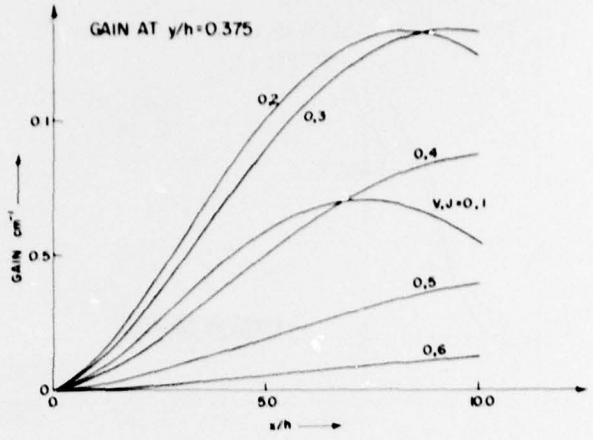

Figure 10

Variation of small-signal gain with flow direction; 1-0 transition, y/h = 0.375.

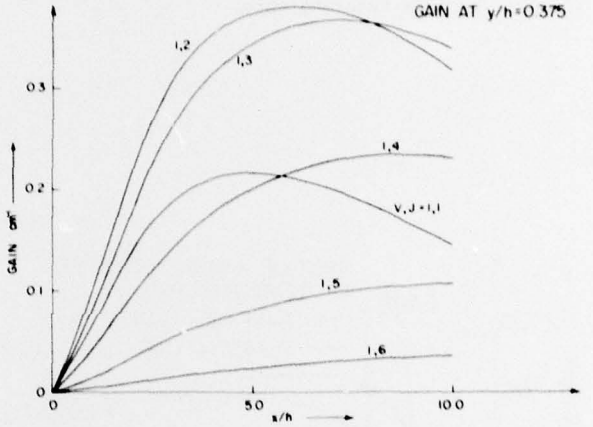

Figure 11

Variation of small-signal gain with flow direction; 2-1 transition, y/h = 0.375.

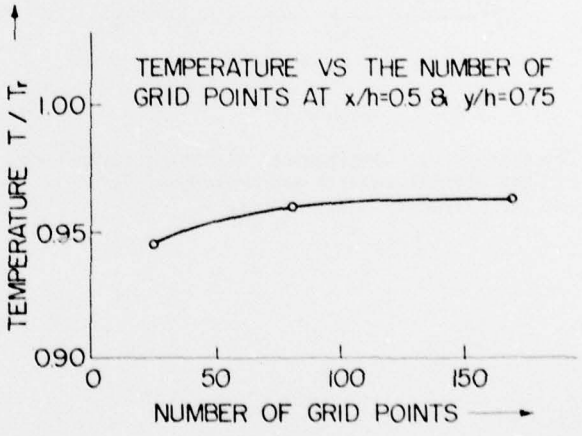

Figure 12

Temperature vs. grid size; a test of convergence properties.

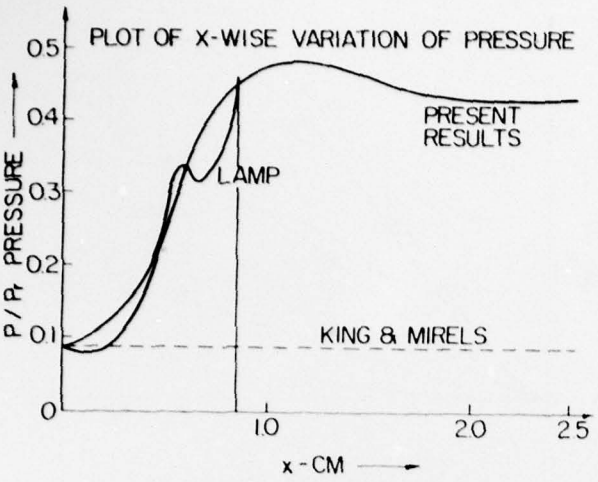

Figure 13

Pressure vs longitudinal distance; comparison between present results and methods of Refs. 18 and 19. Srongly reacting case.

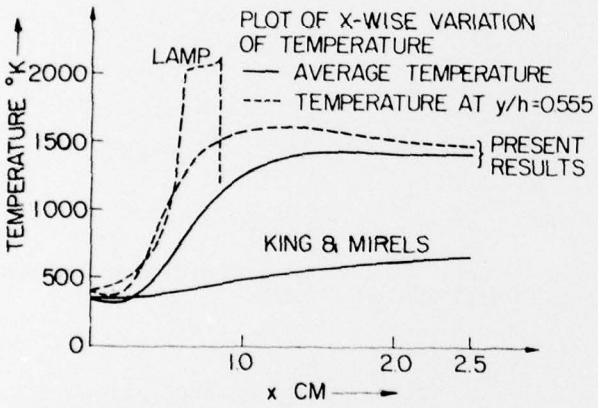

Figure 14

Temperature vs. longitudinal distance; comparison between present results and methods of Refs. 18 and 19. Strongly reacting case.

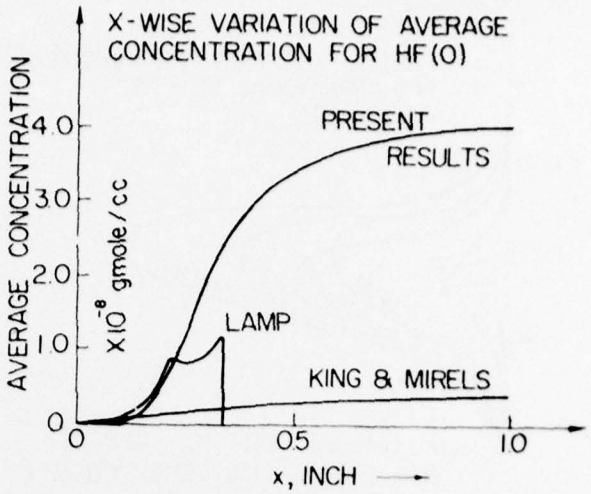

Figure 15

HF(0) density vs longitudinal distance; comparison between present results and methods of Refs. 18 and 19. Strongly reacting case.

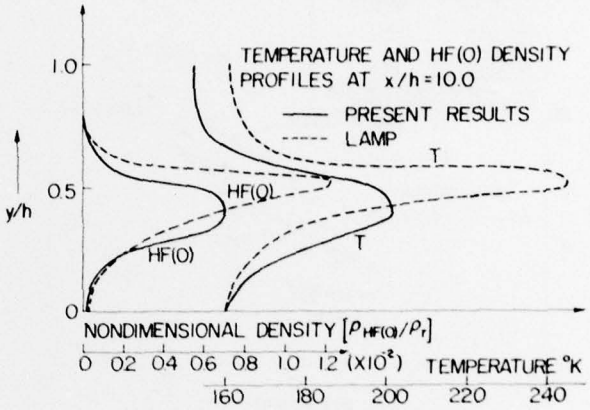

Figure 16

HF(0) and temperature profiles; comparison between present results and methods of Ref. 18. Dilute case.

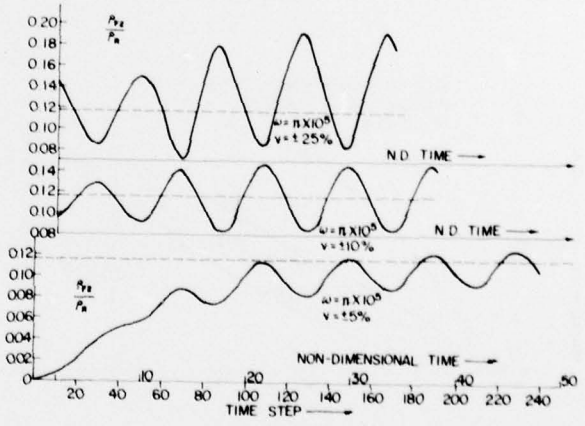

Figure 17

Time wise variation of F_2 density at a given grid point for three different amplitudes.

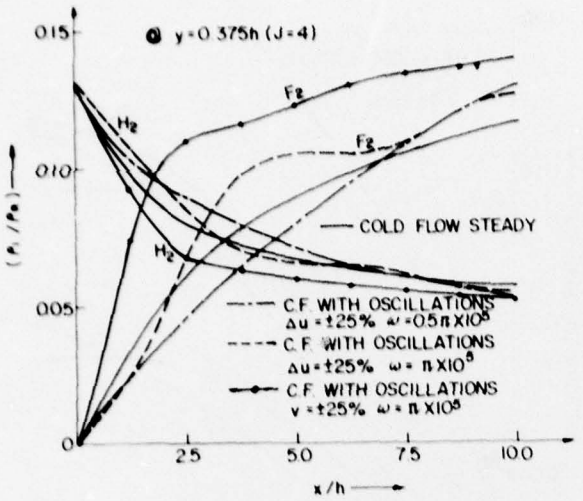

Figure 18

Axial variation of F_2 and H_2 densities for steady and unsteady cases. Cold flow.

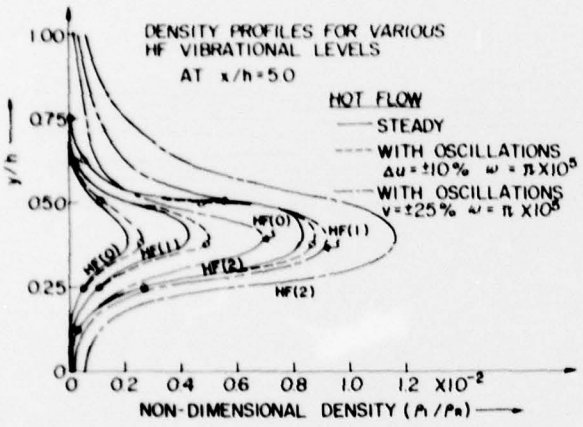

Figure 19

Transverse profiles of several HF vibrational levels; comparison between steady and unsteady flows.

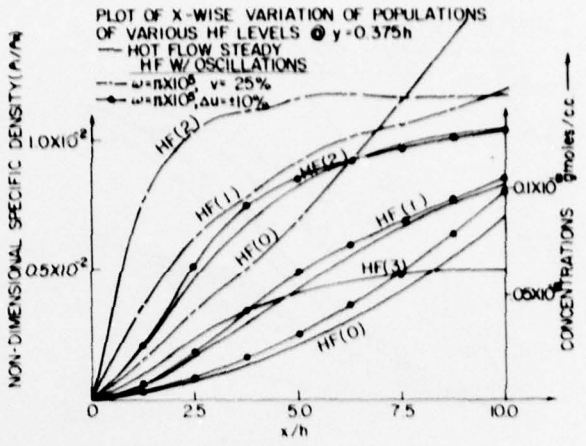

Figure 20

Axial variation of several HF vibrational levels; comparison between steady and oscillating flows.

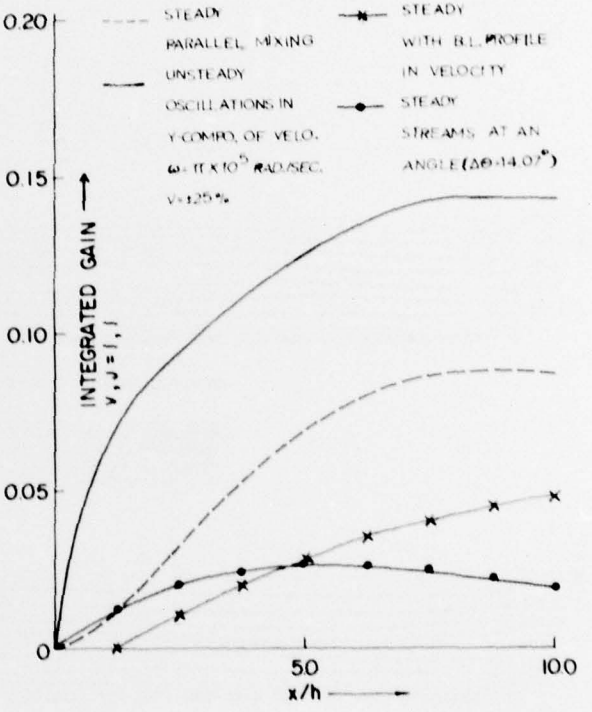

Figure 21

Axial variation of integrated gain; comparison between steady and oscillating flows

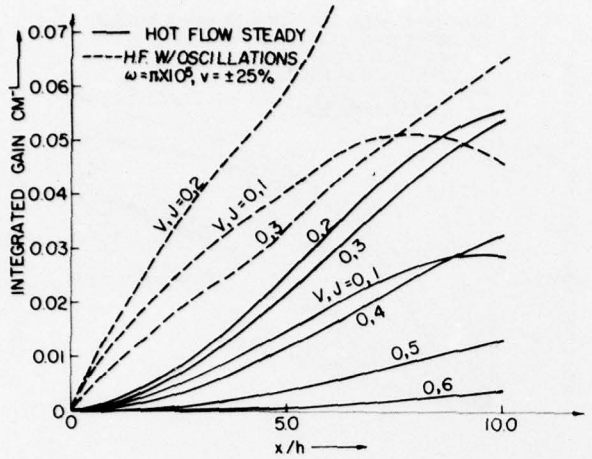

Figure 22

Axial variation of integrated gain; 1-0 transition steady and unsteady flows.

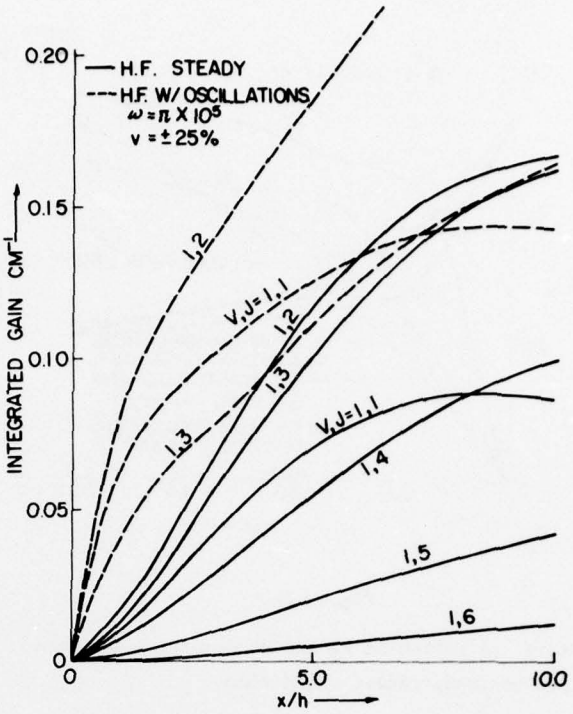

Figure 23

Axial variation of integral gain; 2-1 transition. Steady and unsteady flows.

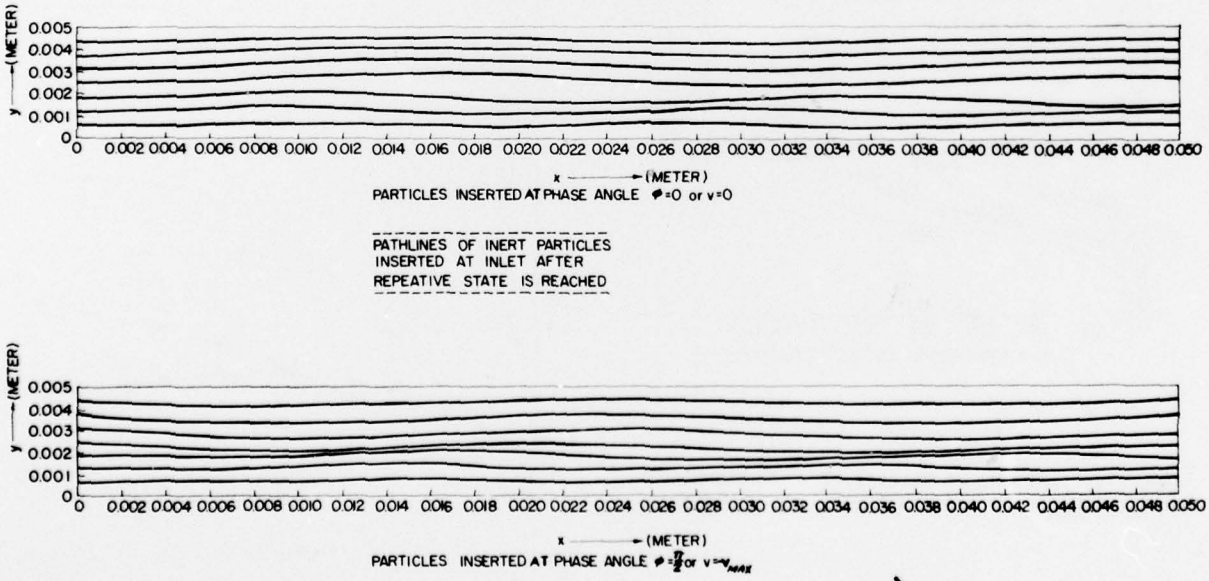

Figure 24

Path lines of given fluid elements in the fluctuating flow. Sinusoidal fluctuations in v velocity at F_2 stream inlet for inert particles inserted at two different phase angles. $w = \pi \times 10^5$ rad./sec. and $v = \pm 25\%$.